In Silico Study of Sensing Performance Functionalized and Decorated Nanocone Toward H_2S Gas

Vessally, Esmail**+; Musavi, Seyed Omid; Amini, Issa; Najafi, Azzatollah; Poor Heravi, Mohammad Reza

Department of Chemistry, Payame Noor University, Tehran, I.R. IRAN

ABSTRACT: *DFT studies were performed to evaluate the interaction between the H_2S gas and the surface of a Carbon NanoCone (CNC) decorated with a boron atom as a chemical sensor. The optimized and electronic characteristics of pristine CNC, H_2S gas, A and B configurations showed that the pristine CNC wasn't a good candidate to sense the H_2S gas and consequently, its electrical properties are changed insignificantly. To improve the properties of the CNC, several strategies were tried: functionalizing by pyridinol (Pyr) and pyridinol oxide (PyrO) and decorated with metals (M= B, Al, Ga, Mg, and Sc). The obtained data demonstrated that promising results were obtained by decorating the CNC with a boron atom. After full optimization, we achieved two stable configurations between the H_2S gas and CNC/B structure (C and D configurations) with E_{ads}= -10.16 and -11.36 kcal/mol using B3LYP/6-311+G(d) level of theory, respectively. The electronic properties of the CNC/B structure are meaningfully changed after the H_2S molecule is adsorbed. According to the calculation, the energy gap between HOMO and LUMO orbitals of C and D configurations is decreased which could be applied to a chemical signal. Eventually, we concluded that the CNC/B structure could be a potential sensor for the detection of H_2S gas, and decorated with boron atoms is a promising strategy.*

KEYWORDS: *Sensor; Decoration; Functionalize; Nanostructure; DFT.*

INTRODUCTION

The Carbon Nanotubes (CNTs) have been discovered [1] and scientists have been interested in their different applications and properties [2,3]. CNTs have been shown to be a favorable material for various applications in electronics, aerospace, automobiles, fuel cells, hydrogen storage, textiles, sensors, and many more [4-7]. In addition to CNTs, Carbon Nanocones (CNCs) have been the subject of research because of their special electronic and mechanical properties [8]. CNCs can be constructed with specific methods from a graphene network, resulting in different geometrical defects at the tips. The open-ended CNC can be established by cutting 1–5 segments of angle 60° from a sheet of graphene and joining the edges made by the cut, with 1–5 pentagons at the apex [9,10]. Because of their unique topology, CNCs have several potential applications [11,12]. Carbon-based electron field emitters have shown good electron field emission properties because of their ability to emit high currents at low electric fields [13]. CNCs have been also ideally suited for use as scanning probe tips and electron field emitters because of their high stiffness and small size [14].

Hydrogen sulfide (H_2S) is a colorless chalcogen-hydride gas and poisonous, corrosive, and flammable, with trace amounts in ambient atmosphere having a characteristic

***** *To whom correspondence should be addressed.*
+ *E-mail: vessally@pnu.ac.ir & vessally@yahoo.com*
1021-9986/2023/3/704-721 18/$/6.08

foul odor of rotten eggs. Hydrogen sulfide is both an irritant and a chemical asphyxiant with effects on both oxygen utilization and the central nervous system. Low concentrations irritate the eyes, nose, throat and respiratory system (e.g., burning/tearing of eyes, cough, shortness of breath). Asthmatics may experience breathing difficulties. Repeated or prolonged exposures may cause eye inflammation, headache, fatigue, irritability, insomnia, digestive disturbances and weight loss [15,16]. Therefore, the need to control the emission of H_2S gas in the atmosphere is obligatory. For this reason, H_2S sensors with an excellent sensitivity and dependability are in great demand. Developing effective gas sensors based on the nanomaterials is of great interest because of their high electronic sensitivity, high surface to volume ratio and other unique properties [17-36]. In the most cases, pristine nanostructures are not sensitive to chemicals and, therefore, the development of novel nanosensors by manipulated structure is of great importance. Using first principle calculations, several studies have investigated interaction between H_2S and carbon nanostructures [37-41]. They have shown that the electronic properties of carbon nanostructures changed in the presence of H_2S. It should be noted that to increase the sensitivity of the sensor, they used the doping method and functionalizing strategy. Herein, we perform a theoretical study on the adsorption and possible detection of H_2S by the CNC. To improve the properties of our candidate sensor, we used several strategies like functionalizing with pyridinol (Pyr) and pyridinol oxide (PyrO) and decorating with some metals (M= B, Al, Ga, Mg, and Sc). The main question that has been explored in this work is how the electronic properties of CNC are sensitive to the presence of H_2S. The method of detection is based on the fact that the adsorption of a gas on the nanostructure may create a change in the electrical conductance which provides an electronic signal.

COMPUTATIONAL SECTION

Geometry optimizations of a CNC, functionalizing with pyridinol (CNC/pyr), pyridinol oxide (CNC/PyrO) and decorated with some metals (M=B, Al, Ga, Mg, and Sc) (CNC/M) with and without the H_2S molecule were performed using the B3LYP functional [42] and the 6-31G(d) basis set at the gas phase as implemented in the GAMESS software [43]. The B3LYP functional has been used for theoretical studied in previous letters [44,45]. After the full optimization and obtained all considered configurations, full optimization using B3LYP/6-311+G(d) are performed for favorable configurations (CNC/B, C and D configurations) to obtain more accurate results. The adsorption energy (E_{ads}) of H_2S gas on the surface of pristine, functionalizing, and decorated CNC has been defined as follows:

$$E_{ads} = E_{(complex)} - E_{(gas)} - E_{(adsorbent)} \quad (1)$$

Where $E_{(complex)}$ is the total energy of complex formed between H_2S gas and adsorbent, and $E_{(gas)}$ and $E_{(adsorbent)}$ referred to the energy of an isolated adsorbent (i.e. CNC, CNC/Py, CNC/PyO, or CNC/M) and H_2S gas, respectively. Natural bond orbitals (NBO) charge analysis, and molecular electrostatic potential (MEP) calculations were using the same level of theory.

In this research, the energy gap (E_g) and Fermi level (E_F) are also calculated. E_g is difference between the energy level of HOMO and LUMO orbitals as defined in Eq. (2):

$$E_g = E_{LUMO} - E_{HOMO} \quad (2)$$

where E_{LUMO} and E_{HOMO} are the energy of HOMO and LUMO. The conventional assumption for a Fermi level (E_F) is in the middle of the energy gap (E_g) of the molecule at 0 K approximately. Total Density of States (TDOS) analysis on the pristine CNC, A, and B configurations, and also TDOS and Partial Density of States (PDOS) analysis on the CNC/B, C, and D configurations were carried out at the same level of theory. All calculations have been done at 298.14 K and 1 atmosphere.

RESULTS AND DISCUSSION

Pristine carbon nanocone (CNC) and H_2S gas geometry optimization

We have focused on a CNC with a cone angle of 108° with a pentagon shape on the apex (Fig. 1), which is the largest angle previously observed experimentally and predicted theoretically [8,10]. The pristine CNC consists of 80 carbon atoms and the dangling bonds of CNC are saturated with hydrogen atoms. Several types of C-C bonds are observed in CNC with different lengths related to the carbon of the pentagonal and hexagonal rings, respectively (See Fig. 1). The electronic properties of CNC are also studied. The obtained frontier molecular orbital energies (HOMO and LUMO) and the computed energy gap (E_g) values for the considered CNC are shown in Table 1.

Table 1: Adsorption energy (E_{ads}), Energy of HOMO and LUMO orbitals, energy difference of HOMO and LUMO orbitals (E_g), Fermi level energy (E_{FL}), the change of energy gap of nanocone after adsorption(ΔE_g(%)), bipolar moment (DM), working function (Φ), the change of working function of nanocone after adsorption ($\Delta\Phi$), Charge transfer from molecule to nanocone (Q_T), and electron transfer number (ΔN) for H_2S molecule, carbon nanocone (CNC), A and B configurations at the theoretical level of B3LYP/6-31G(d).

Systems	E_{ads} (kcal/mol)	E_{HOMO} (eV)	E_{FL} (eV)	E_{LUMO} (eV)	E_g (eV)	$\%\Delta E_g$	DM (Debye)	Φ (eV)	ΔΦ (eV)	Q_T (me)	ΔN
H_2S	-	-7.12	-3.29	0.53	7.65	-	1.43	3.29	-	-	-
CNC	-	-5.01	-3.80	-2.59	2.43	-	5.54	3.80	-	-	-
A	-0.99	-5.06	-3.86	-2.65	2.41	-0.55	7.22	3.86	0.06	5	0.06
B	41.73	-5.02	-3.79	-2.57	2.45	1.01	5.24	3.79	0.01	0.1	0.05

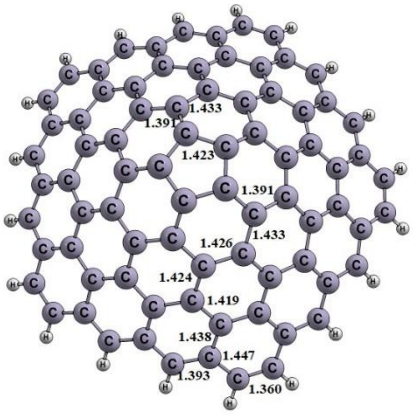

(a)

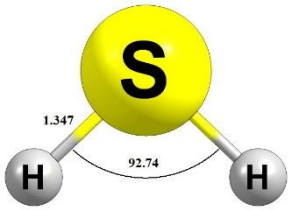

(b)

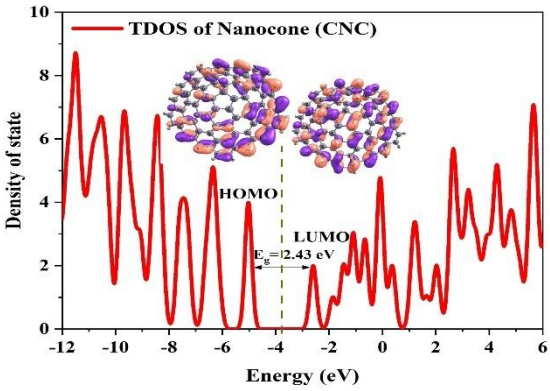

Fig. 1: Optimized structure of (a) CNC (b) H_2S gas, and (c) total density of states (TDOS of CNC (The dashed line in TDOS plots indicates E_F. All distances are in Å).

Fig. 1c represents the CNC TDOS with an energy gap of 2.43 eV. Our results are in good agreement with the previous study [46]. The graphical presentation of the HOMO and LUMO distribution of pristine CNC is presented in Fig. 1c, too. The optimized structure of the H_2S gas is depicted in Fig. 1b.

H_2S adsorption on the pristine CNC

To determine the minimum energy adsorption structure of H_2S gas on the exterior and interior surface of the considered CNC, several distinct starting structures were used for optimization, including the hydrogen and sulfur heads of H_2S being on top of the ring center or close

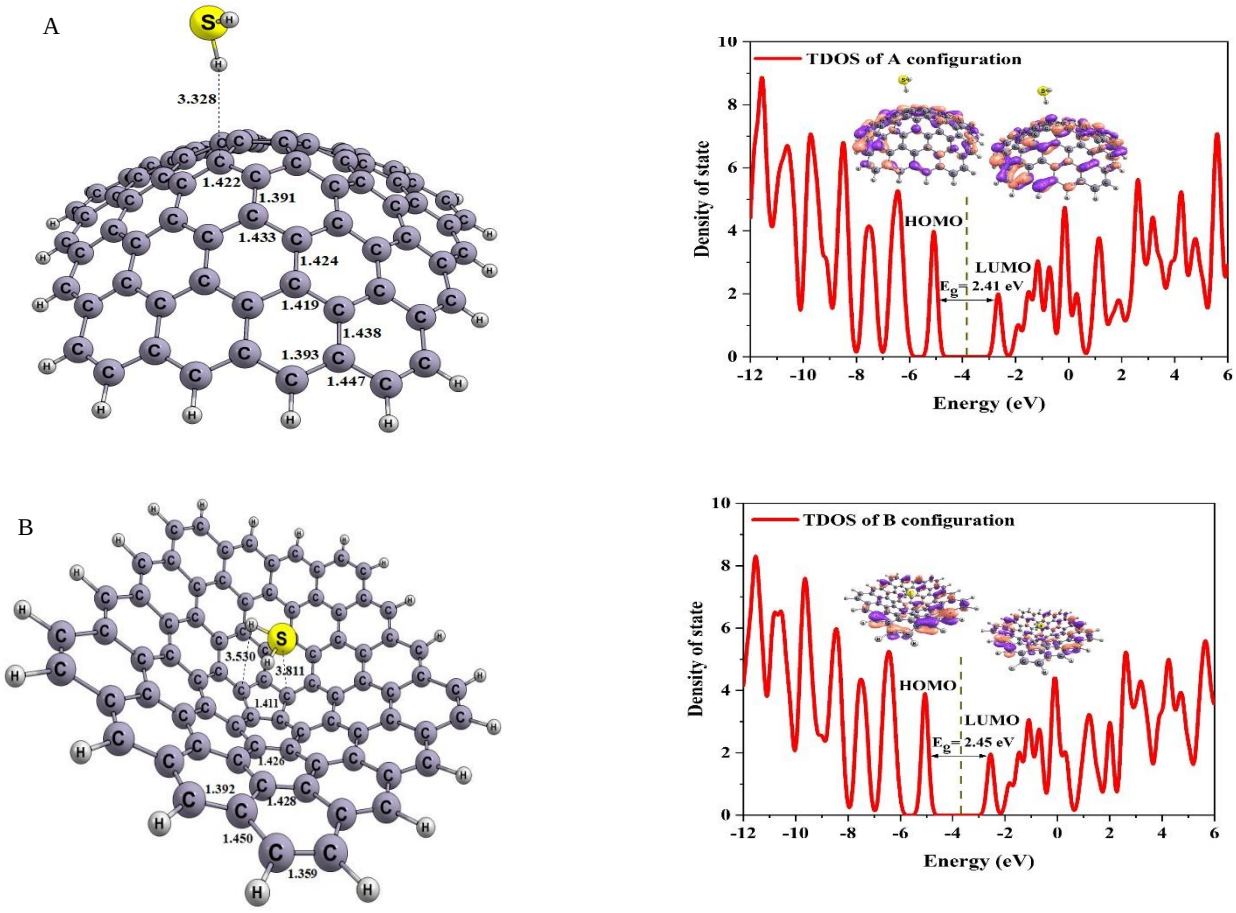

Fig. 2: The optimized structures, and TDOS plots of stable adsorption configurations of H_2S on the outside and inside of CNC (A and B configurations). All distances are in Å. The dashed line in TDOS plots indicates E_F.

to a carbon atom. Also, we have examined the initial configurations in which the H-S bond has been placed parallel to C-C bonds. During the full optimization, H_2S has reoriented so that its H atom gets closer to one of the C atoms in the pentagon ring of the CNC. After geometry optimization, it was found that only two configurations are stable (Fig. 2). In Table 1, we have summarized our results for E_{ads}, charge analysis, and E_g.

The calculated E_{ads} values for two obtained configurations using Eq. (1) are listed in Table 1. As shown in Table 1, E_{ads} values for A and B configurations are -0.99 and 41.73 kcal/mol, respectively indicating very weak physical adsorption they are energetically unfavorable. The C-H distance in the A configuration is 3.32 Å and in the B configuration is 3.53 and 3.81 Å (see Fig. 2). As depicted in Table 1, the adsorption of H_2S gas on the outside and inside of CNC is along with a partial charge transfer process (about 5 and 0.1 |me| for A and B configurations, respectively). The obtained results confirmed that the weak electrostatic interaction between H_2S and CNC is occurred, and the pristine CNC is not a favorable sensor for sensing and detecting H_2S gas.

The electronic properties of the A and B configurations were calculated to investigate the effect of adsorption H_2S on the electronic properties of pristine CNC. As it can be obtained from Table 1, the E_g and E_F show a small change after adsorption process. The results indicated the E_g in the A and B configurations are 2.41 and 2.45 eV, respectively. The small shift of E_g ($\%\Delta E_g$) is depended to the weak adsorption on the exterior and interior surface of pristine CNC. The TDOS and graphical visualization of the HOMO and LUMO are analyzed and depicted in Fig 2. According to this figure, there is no significant difference between A and B configurations and pristine CNC which is confirms the weak interactions between the H_2S gas and CNC.

The value of the electron transfers number (ΔN) is calculated using the following equation:

$$\Delta N = \frac{\mu_{H_2S} - \mu_{Complex}}{2\left(\eta_{H_2S} + \eta_{Complex}\right)} \quad (3)$$

In this equation, $\mu_{(Complex)}$ represents the chemical potential for complex between H_2S gas and adsorbent, μ_{H_2S} represents the electrical chemical potential for the H_2S gas, $\eta_{(Complex)}$, the chemical hardness for complex between H_2S gas and adsorbent and η_{H_2S} is the chemical hardness for the H_2S gas. It should be noted that the electrical chemical potential measures the tendency of the electron to deflect which is related to the size of the atoms and ions and the ease of deflection of the electron density. The value of the electron transfer number ΔN is positive for all absorption sites that implies that the electron transfer carried out from the H_2S gas to the A and B configurations.

In the electronics industry, controlling the work function of materials is considered as one of the key tasks to improve the performance of the device. The work function of nanomaterials is one of the most important properties to control the surface properties. The work function changes related to charge transfer between the adsorbent (pristine CNC) and the adsorbing (H_2S gas) have been studied. The work function for a semiconductor molecule is the minimum amount of energy required to lift an electron from the Fermi surface to a point far enough away that it is not affected by the material. However, the current density of electrons emitted in a vacuum is theoretically described by the following classical equation:

$$j = AT^2 \exp\left(\frac{-\Phi}{kT}\right) \quad (4)$$

Which is called Richardson's constant $^{A}/_{m^2}$, T is the temperature (K) and Φ (eV) are the function of a substance. The numerical value Φ is calculated using the following equation:

$$\Phi = E_{inf} - E_{FL} \quad (5)$$

That E_{inf} is the electrostatic potential at infinity and E_{FL} are Fermi level energy. Here the electrostatic potential at infinity is assumed to be zero. The calculated values of the function Φ using equation (5) for the CNC nanostructure when interacting with the H_2S molecule are given in Table 1. The DFT calculations clarified that the calculated the Φ values of the pristine CNC nanostructure changed after the adsorption of the H_2S gas. According to Equation (4), the electron diffusion current density depends exponentially on the negative value. As the Φ and Fermi level of CNC are not changed sensibly, the current density slowly altered when the H_2S gas absorbed on the exterior and the interior surface of CNC, indicating a little sensitivity of the adsorbents to the presence of the H_2S gas. The ΔΦ values of A and B indicated that pristine CNC can't play as a Φ-type sensor due to weak absorption energy.

The interaction between the H_2S and CNC may alter the electronic structure of the CNC, which could be reflected by the change in the electrical conductance of the CNC. The conduction electron population of a semiconductor which is the responsible of electrical conductivity is given by [427]

$$\sigma = AT^{3/2}\exp\left(-E_g / 2kT\right) \quad (6)$$

Where *A* (electrons/$m^3K^{3/2}$) is a constant, and *k* is the Boltzmann's constant. As mentioned before, a chemical sensor works based on the change in its electrical conductivity after the adsorption process. It has been previously [47] shown that this relation works well for determining the sensitivity of a detector based on the change of E_g.

Manipulating the structure to improve reactivity and sensitivity

Functionalizing with Pyr and PyrO

One of the main ways to regulate the properties of the nanomaterials is using chemical functionalization. Indeed, recent experiments have shown that the electronic properties of carbon nanostructures can be controlled to fit the requirements of specific applications by chemical bonding of a molecule or a chemical element to the pristine material [48]. *Bekyarova et al.* [49] have synthesized Pyr functionalized CNTs (CNT-$COOC_5H_4N$) and explored the change of their electronic properties on exposure to HCl. They found that the CNT-$COOC_5H_4N$ films exhibited a decrease in resistance in the presence of HCl and can be used HCl chemical sensors. Herein, to overcome the problem of insensitivity of the CNC we employed the same strategy and use Pyr and PyrO to functionalize pristine CNC. To this aim, we functionalized the CNC at its tip (See Figs. 3 and 4). As shown in Table 2, after functionalization of the CNC with the Pyr and PyrO groups, the HOMO partially

Table 2: Adsorption energy (E_{ads}), Energy of HOMO and LUMO orbitals, energy difference of HOMO and LUMO orbitals (E_g gap), Fermi level energy (E_{FL}), and the change of energy gap of nanocone after adsorption(ΔE_g(%)) for carbon nanocone functionalized with Pyridinol group (CNC/Pyr), S1, S2, S3, and Pyridinol oxide group (CNC/PyrO), S4, S5, and S6 configurations at the theoretical level of B3LYP/6-31G(d).

Systems	E_{ads} (kcal/mol)	E_{HOMO} (eV)	E_{FL} (eV)	E_{LUMO} (eV)	E_g (eV)	$\%\Delta E_g$
CNC/Pyr	-	-4.77	-3.76	-2.75	2.026	-
S1	-4.31	-4.86	-3.85	-2.84	2.020	-0.29
S2	-2.37	-4.86	-3.86	-2.86	2.008	-0.90
S3	-2.17	-4.81	-3.80	-2.79	2.012	-0.67
CNC/PyrO	-	-4.84	-3.83	-2.82	2.021	-
S4	-4.31	-4.90	-3.90	-2.90	2.006	-0.77
S5	-2.08	-4.84	-3.83	-2.82	2.020	-0.07
S6	-2.05	-4.85	-3.84	-2.83	2.021	0

shifts to the higher energies and LUMO slightly moves to the upper energies, and then it causes the gap energy to be shorter than pristine CNC (E_g= 2.026 and 2.021 eV for CNC/Pyr and CNC/PyrO, respectively). After we had obtained the stable structures of CNC/Pyr and CNC/PyrO, we investigated the position of H_2S gas on the functional groups as shown in Fig. 3 and 4. After optimization of considered structures, we got three configurations of interaction between CNC/Pyr and H_2S gas (S1, S2, and S3) and CNC/PyrO and H_2S gas (S4, S5, and S6). In the experimental work, the functionalized CNTs will undergo protonation, which is the strongly acidic character of HCl. In accordance, here the charged conjugate acid is the predicted structure of the H_2S adsorbed CNC/Pyr and CNC/PyrO (See Fig. 3, and 4). From Table 2, the E_g of obtained configurations are in the range of 2.006 to 2.021 eV, which indicates a small shift of E_g via the adsorption process due to the weak adsorption on the CNC/Pyr and CNC/PyrO structures. The computed E_{ads} values for S1-S6 configurations are listed in Table 2.

It could be realized from this table, negative values of adsorption energy display the structures are stable though the interaction between H_2S gas and considered adsorbent is weak. The interaction distance in achieved configurations also confirms the weak interactions. In summary, there are two important parameters including E_{ads} and E_g, in the gas sensing potential by nanoparticles. In This case, E_{ads} and E_g of adsorption of the H_2S gas over to CNC/Pyr and CNC/PyrO structures are very low, and consequently, these adsorbents aren't good and sensitive sensors for detecting H_2S gas.

Decorated with metals (M= B, Al, Ga, Mg, and Sc)

To enhance the interaction between the adsorbing molecule and the host adsorbent, decorating with alkali metals, alkaline earth, element of group III, and Transition Metals (TM) opens a new strategy in this field recently [50-53]. In light of this idea, we used this strategy to increase adsorption energy and remarkable change in electronics to introduce CNC as a sensor for detecting H_2S gas. For this aim, pristine CNC was decorated at its tip with B, Al, Ga, Mg, and Sc metals to survey optimized structures and electronic properties of achieved structures. Optimized structures of CNC/M (M=B, Al, Ga, Mg, and Sc) were depicted in Figs. 5-9. The distance of C-M interaction is about 2.24 to 3.05 Å. The stabilization of the considered structures was obtained as follows and summarized in Tables 3 and 4:

$$E_{stab} = E_{CNC/M} - E_{CNC} - E_M \quad (7)$$

Where $E_{CNC/M}$ represents the total electronic energy of the CNC/M structure. E_{CNC} and E_M are the total electronic energy of isolated pristine CNC and the M atom, respectively. From those tables, the E_{stab} values range from -6.38 to -54.44 kcal/mol, which indicates our structures are very stable.

The electronic properties of CNC/M structures are also checked; the E_{HOMO}, E_{LUMO}, E_F and E_g values for these mentioned structures are tabulated in Table 3 and 4. Our results display that the E_g of these structures has changed compared to the pristine CNC. It can be seen in the results, the HOMO and LUMO levels shifted towards upper energy levels (except the LUMO level of CNC/Mg structure) and lead to increase E_g for CNC/B, CNC/Al, and CNC/Ga, and decrease E_g for CNC/Mg and CNC/Sc.

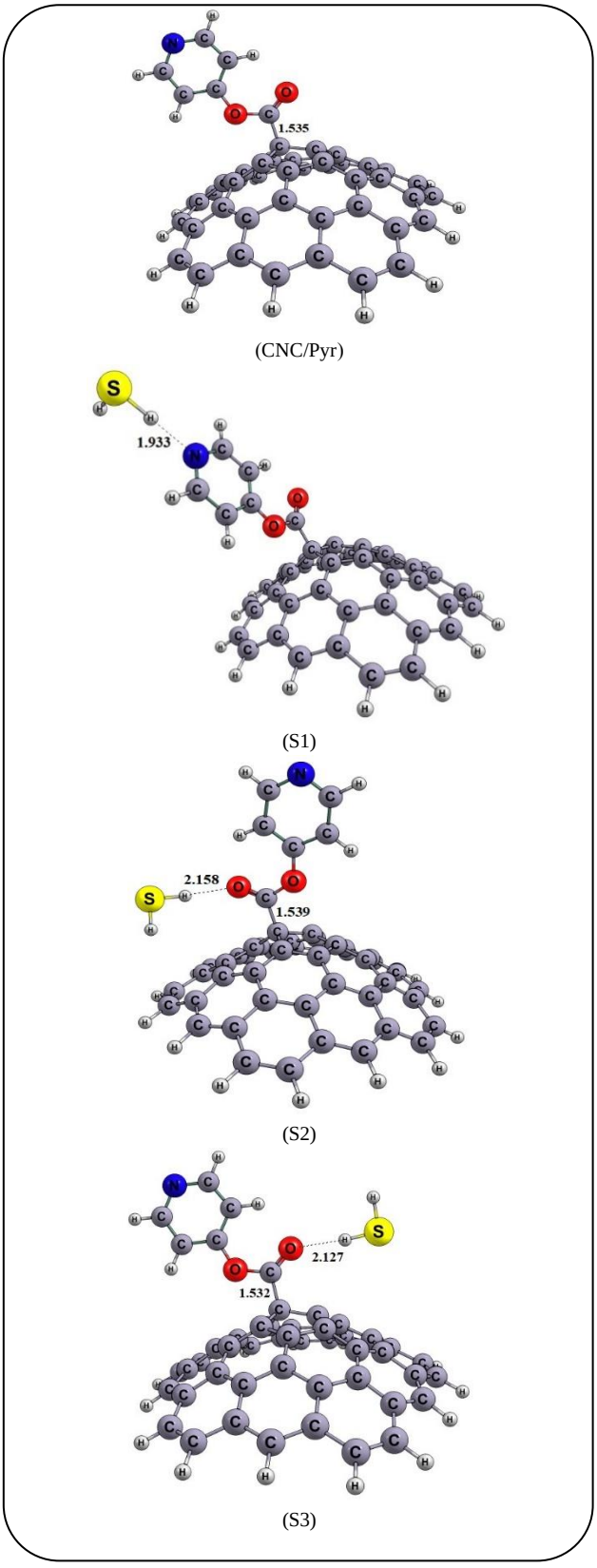

Fig. 3: Optimized structures of the CNC/Pyr, S1, S2, and S3 configurations (Bonds are in Å).

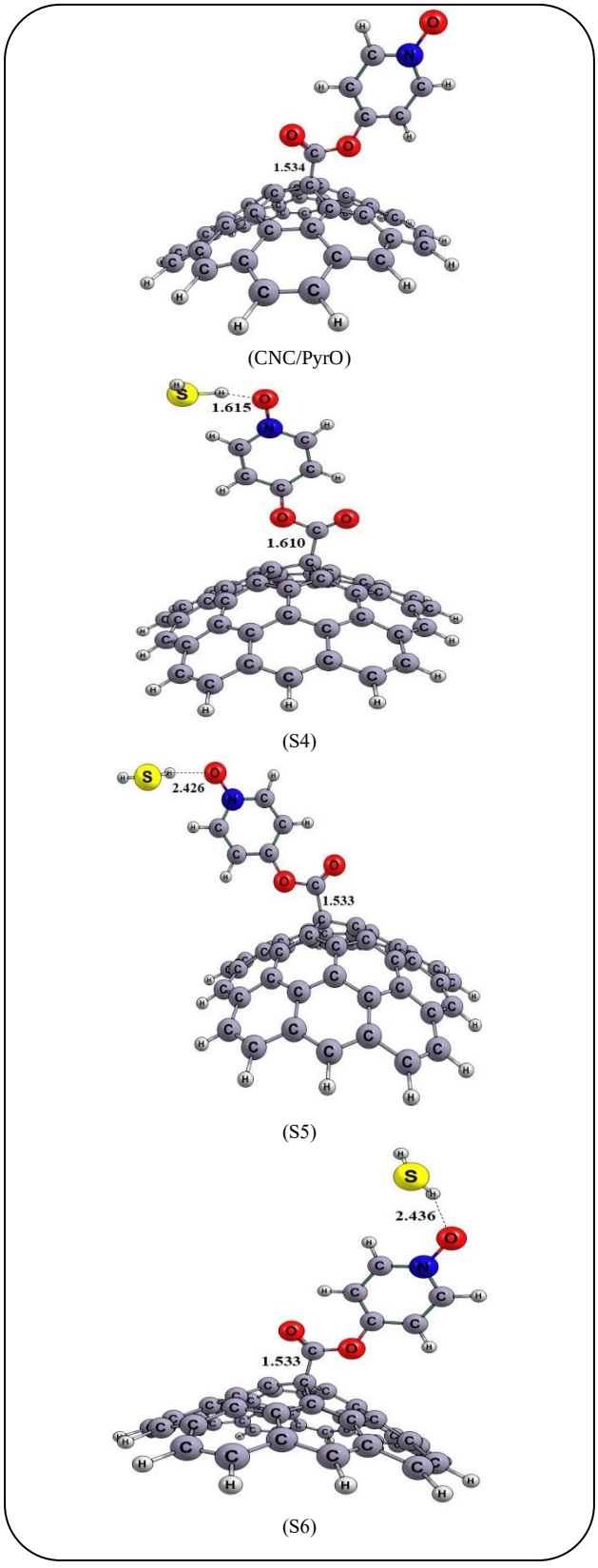

Fig. 4: Optimized structures of the CNC/PyrO, S4, S5, and S6 configurations (Bonds are in Å).

Table 3: Adsorption energy (E_{ads}), Energy of HOMO and LUMO orbitals, energy difference of HOMO and LUMO orbitals (E_g gap), Fermi level energy (E_{FL}), and the change of energy gap of nanocone after adsorption (ΔE_g(%)) for carbon nanocone decorated with some metals (CNC/M, M=Sc, Al, Ga, and Mg), their configurations at the theoretical level of B3LYP/6-31G(d).

Systems	E_{ads} (kcal/mol)	E_{HOMO} (eV)	E_{FL} (eV)	E_{LUMO} (eV)	E_g (eV)	%ΔE_g
CNC/Sc	-	-4.03	-3.17	-2.31	1.72	-
S7	-74.47	-4.97	-3.73	-2.49	2.49	44.9
CNC/Al	-	-4.78	-3.24	-1.70	3.082	-
S8	-0.14	-4.86	-3.32	-1.78	3.079	-0.10
S9	0.16	-4.73	-3.19	-1.65	3.078	-0.13
CNC/Ga	-	-4.72	-3.22	-1.72	3.00	-
S10	-2.96	-4.65	-3.23	-1.80	2.848	-5.07
S11	-1.63	-4.65	-3.16	-1.67	2.979	-0.70
S12	-1.12	-4.79	-3.30	-1.81	2.980	-0.67
CNC/Mg	-	-4.68	-3.71	-2.74	1.94	-
S13	-4.09	-4.53	-3.40	-2.27	2.26	16.5

In order to check more closely, the total density of state (TDOS) and partial density of state (PDOS) of CNC/B structure illustrated in Fig. 9. Per this figure, decorated CNC with B atom leading to new HOMO and LUMO with the upper level compared to pristine CNC, hence the E_g between HOMO and LUMO increased. The results of PDOS showed that the B atom is especially responsible for creating the new LUMO level. Therefore, the decorated CNC with metals can affect the electronic properties of pristine CNC.

In the following, we inspect the H_2S adsorption on the CNC/M structures in the decorated part. Our results of obtained configurations represented in Fig. 5-8, and 10, at which the H and S of H_2S gas is interact with M atom of the CNC/M structures. The computed E_{ads} values for obtained structures using Eq. (1) are listed in Tables 3 and 4. From Table 3, the formed structures are divided into three categories: one of them, S7 (configuration from an interaction between CNC/Sc and H_2S gas), is very stable. Due to the bond between H-S being broken and forming a new bond between H-Sc and S-Sc, it isn't suitable for use as a sensor. The second category includes configurations that have very weak adsorption energy. S8-S13 configurations in Table 3 are included in this category. As shown in this table, the E_g for these configurations ranges between 0.16 to -4.09 kcal/mol, which confirms the weak physical adsorption of H_2S gas on the exterior surface of CNC/M. The interaction distance between H or S from H_2S gas and M from CNC/M is about 2.86-3.87 Å which indicate the weak interaction between them. Finally, the third category gives the best and most desirable configuration. The C and D configurations are of this category (See Fig. 10). In these configurations, the H and S atoms of H_2S gas interacted with the B atom of CNC/B, the H-B, and S-B distances are 2.47 and 2.56 Å, respectively. The calculated E_{ads} values for C and D configurations based on Eq. (1) are -9.09 and -6.29 kcal/mol, respectively (See Table 4). Negative values of the E_{ads} demonstrate that these configurations are stable, and also the interaction between H_2S gas and CNC/B is a physisorption process. According to our results, it is obvious that the adsorption process in the C configuration is stronger than in the D configuration. It means that the B···H is stronger than S···B. Natural bond orbital analysis (NBO) showed that charge transfer occurred after the adsorption process, too. According to the listed results in Table 4, 44 |me| transferred from H_2S to CNC/B, while 179 |me| transferred from CNC/B to the H_2S gas. This fact confirmed the physisorption interaction.

In order to complete our studies, we focused on the electronic properties like E_{HOMO}, E_{LUMO}, and E_g to explain important parameters about the molecules. As we seen in Table 3, the change of the E_g S7 compared to CNC/Sc is

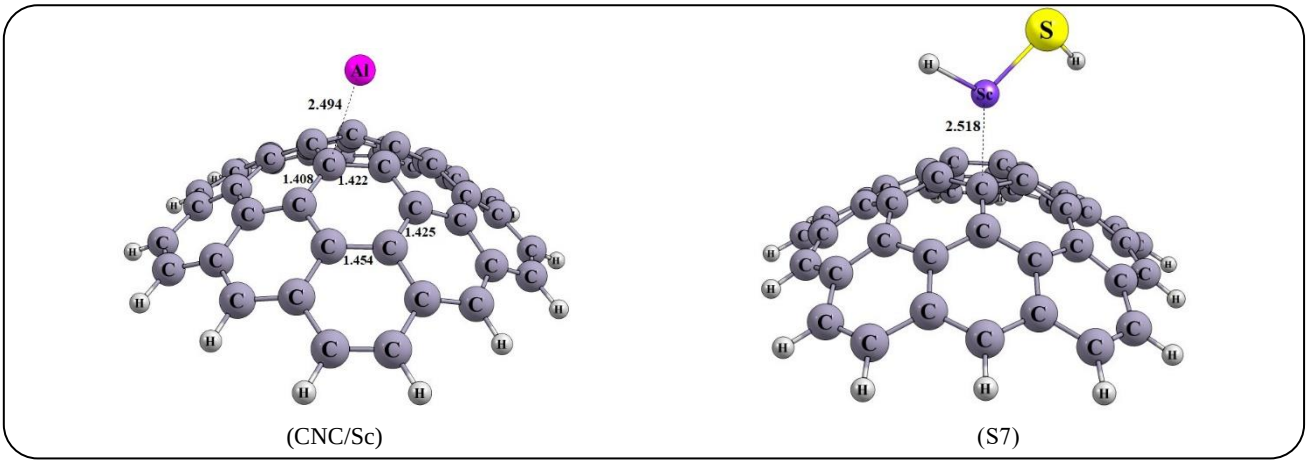

(CNC/Sc) (S7)

Fig. 5: Optimized structures of the CNC/Sc and S7 configuration (Bonds are in Å).

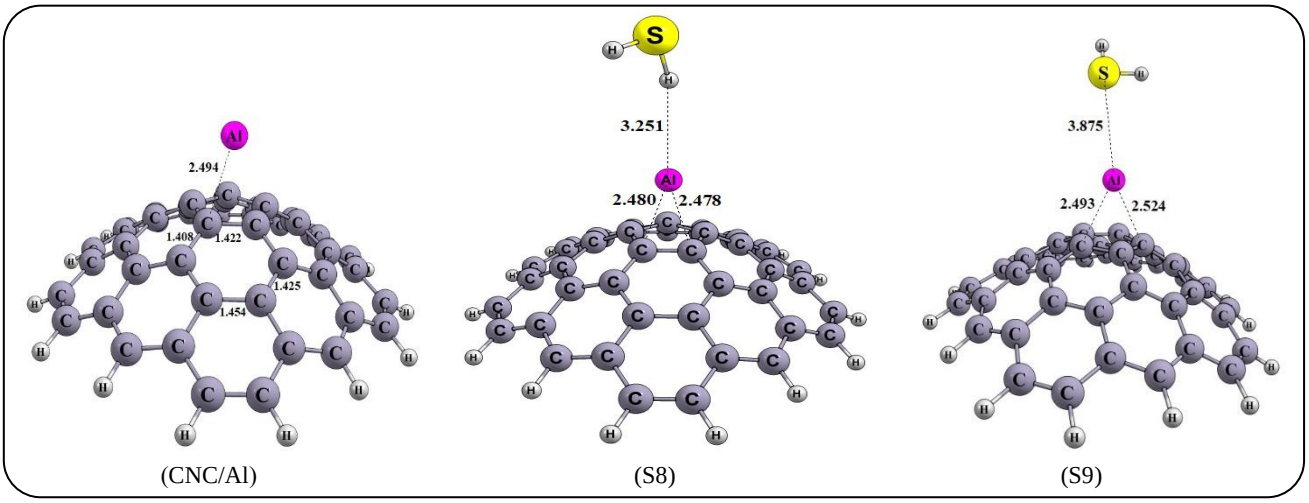

(CNC/Al) (S8) (S9)

Fig.6: Optimized structures of the CNC/Al, S8 and S9 configurations (Bonds are in Å).

very significant (%ΔE= 44.9) which confirmed the strong adsorption. The new HOMO and LUMO levels in downwards compared to the CNC/Sc are responsible for a significant change of the E_g. About other configurations in Table 3, we see slight change in the E_g related to the CNC/M. The small shift of E_g (%ΔE) is related to the weak adsorption on the exterior surface of CNC/M. Eventually, we survey to the electronic properties of C and D configurations (See Table 4). TDOS, PDOS, and visualization of HOMO and LUMO of C and D configurations are displayed in Fig. 10. From obtained results, there is a remarkable change between considered configurations and CNC/B that is related to the physisorption process. From PDOS spectra, there are new LUMO and HOMO levels because of the interaction between H_2S gas and CNC/B which is B atom more involved. Also from TDOS plots their valance and conduction levels in both the C and D configurations notably shift upwards and downwards, respectively, therefore, the E_g value of the CNC/B is notably decreased by %26.24 and %25.42, respectively. Thus, CNC/B structure can be a good candidate for physisorption sensing H_2S gas.

The ΔN values of our configurations are positive (0.05 and 0.02 for C and D configurations, respectively) which implies that the electron transfer carried out from the H_2S gas to the CNC/B structures. From Table 2, ΔΦ of C and D configurations are 0.37 and 0.13, respectively, which indicate higher sensing ability. However, it can be suggested the CNC/B can be play as a Φ-type sensor due to physical adsorption energy and low recovery time.

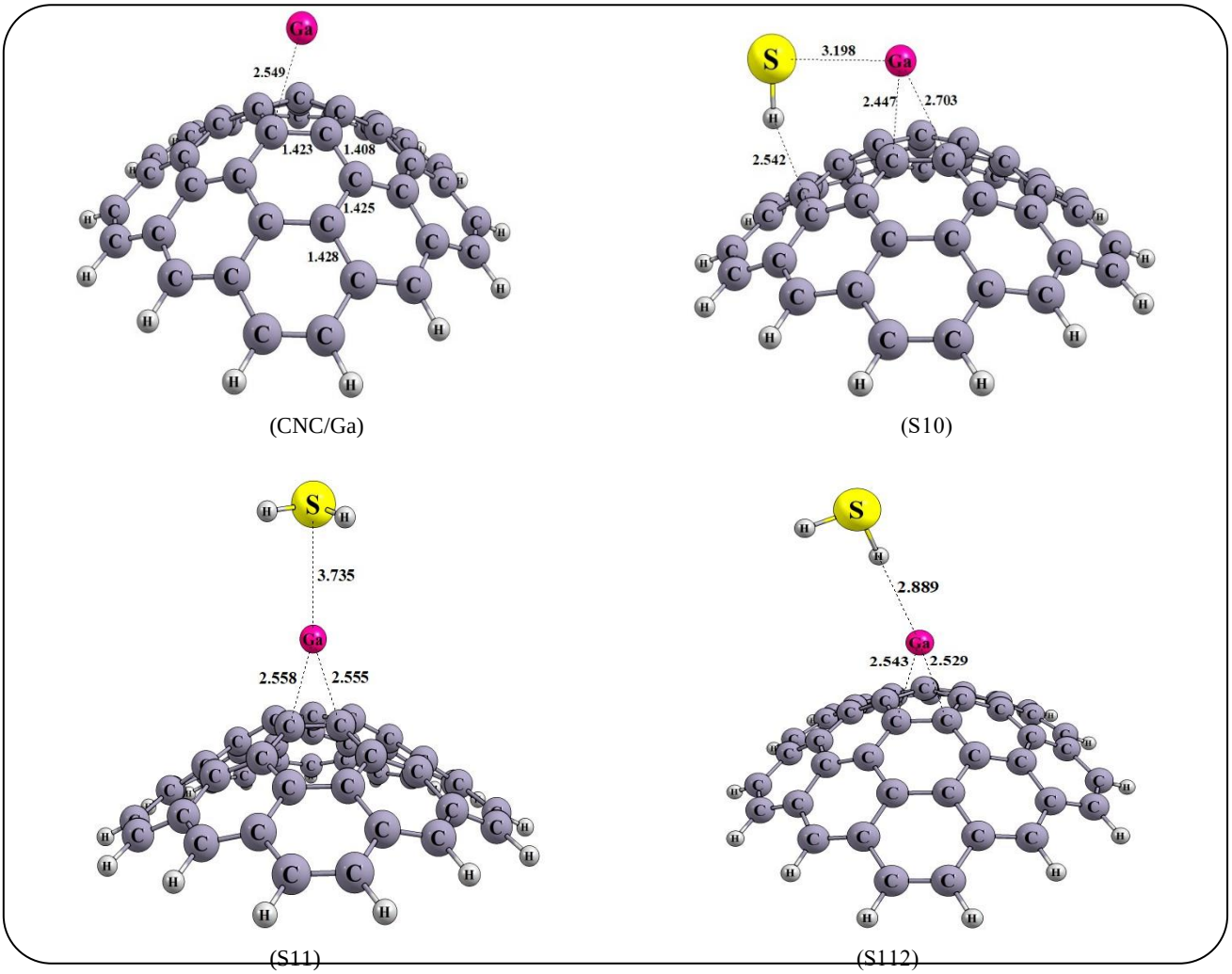

Fig. 7: Optimized structures of the CNC/Ga, S10, S11 and S12 configurations (Bonds are in Å).

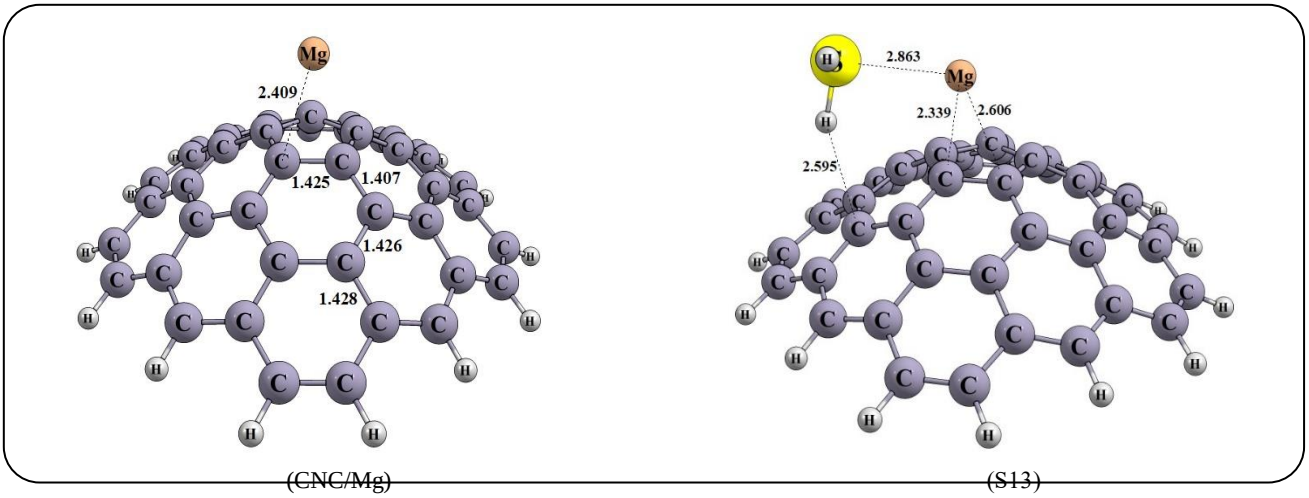

Fig. 8: Optimized structures of the CNC/Mg, and S13 configurations (Bonds are in Å).

Table 4: Adsorption energy (E_{ads}), Energy of HOMO and LUMO orbitals, energy difference of HOMO and LUMO orbitals (E_g), Fermi level energy (E_{FL}), the change of energy gap of nanocone after adsorption(ΔE_g(%)), bipolar moment (DM), working function (Φ), the change of working function of nanocone after adsorption (ΔΦ), Charge transfer between nanocone and molecule (Q_T), and electron transfer number (ΔN) for carbon nanocone decorated with B atom (CNC/B), C and D configurations at the theoretical level of B3LYP/6-31G(d) and B3LYP/6-311+G(d).

Systems	E_{ads} (kcal/mol)	E_{HOMO} (eV)	E_{FL} (eV)	E_{LUMO} (eV)	E_g (eV)	%ΔE_g	DM (Debye)	Φ (eV)	ΔΦ (eV)	Q_T (me)	ΔN
6-31G(d)											
CNC/B	-	-4.92	-3.40	-1.88	3.03	-	4.06	3.40	-	-	-
C	-9.09	-4.89	-3.77	-2.65	2.24	-26.24	7.64	3.77	0.37	-44	0.05
D	-6.29	-4.66	-3.53	-2.40	2.26	-25.42	3.48	3.53	0.13	179	0.02
6-311+G(d)											
CNC/B	-	-5.29	-3.77	-2.25	3.04		5.25	3.77	-	-	-
C	-10.16	-5.22	-4.11	-3.00	2.22	26.97	8.36	4.11	0.34	85	0.04
D	-11.36	-4.95	-3.85	-2.76	2.19	27.96	4.24	3.85	0.09	234	0.01

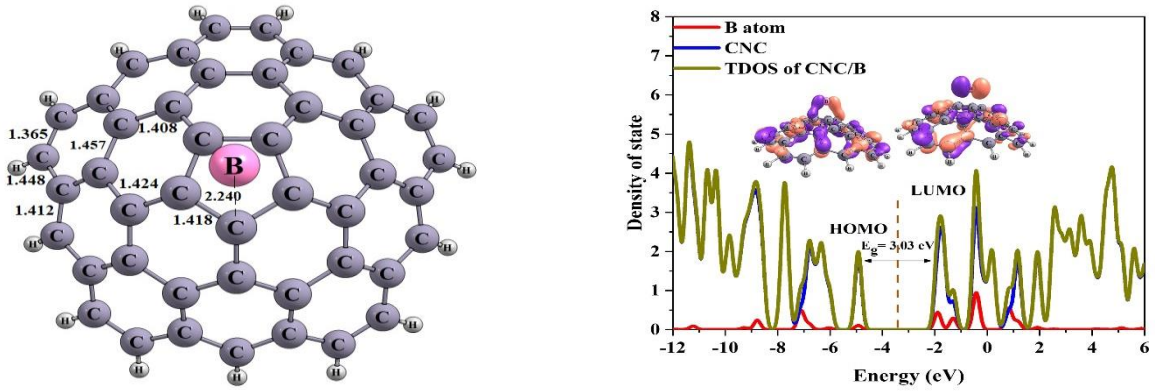

Fig. 9: The optimized structures, TDOS, and PDOS plots of stable structure of the CNC/B. All distances are in Å. The dashed line in PDOS plots indicates E_F.

To obtain accurate data, we performed new calculations on the CNC/B structure and C and D configurations *via* B3LYP/6-311+G(d) level. Our results reported in Table 4 and Fig. 11. From this table, it is clear that the E_{ads} and E_g are increased and decreased, respectively. After full optimization with B3LYP/6-311+G(d) level, E_{ads} of C and D configurations changed to the -10.16 and -11.36 kcal/mol which is higher than B3LYP/6-31G(d) level. On the other hand, H···B in C configuration increased to 2.59 Å and the S···B distance decreased to 2 Å with the new basis set. The E_g of CNC/B isn't a significant difference between the two methods and their values are close. But the E_g of C and D configurations in the 6-311+G(d) basis set are narrower than and the %ΔE_g is bigger than the 6-31G(d) basis set. The TDOS and PDOS of CNC/B structure, C, and D configurations are confirmed in our data. Although, the results of the two basis functions are slightly different. Nevertheless the results of both of them confirm each other.

NCI (non-covalent interaction) and RDG (reduced-density gradient) analysis

The NCI analysis gives useful information about the non-covalent interaction within a molecule [54].

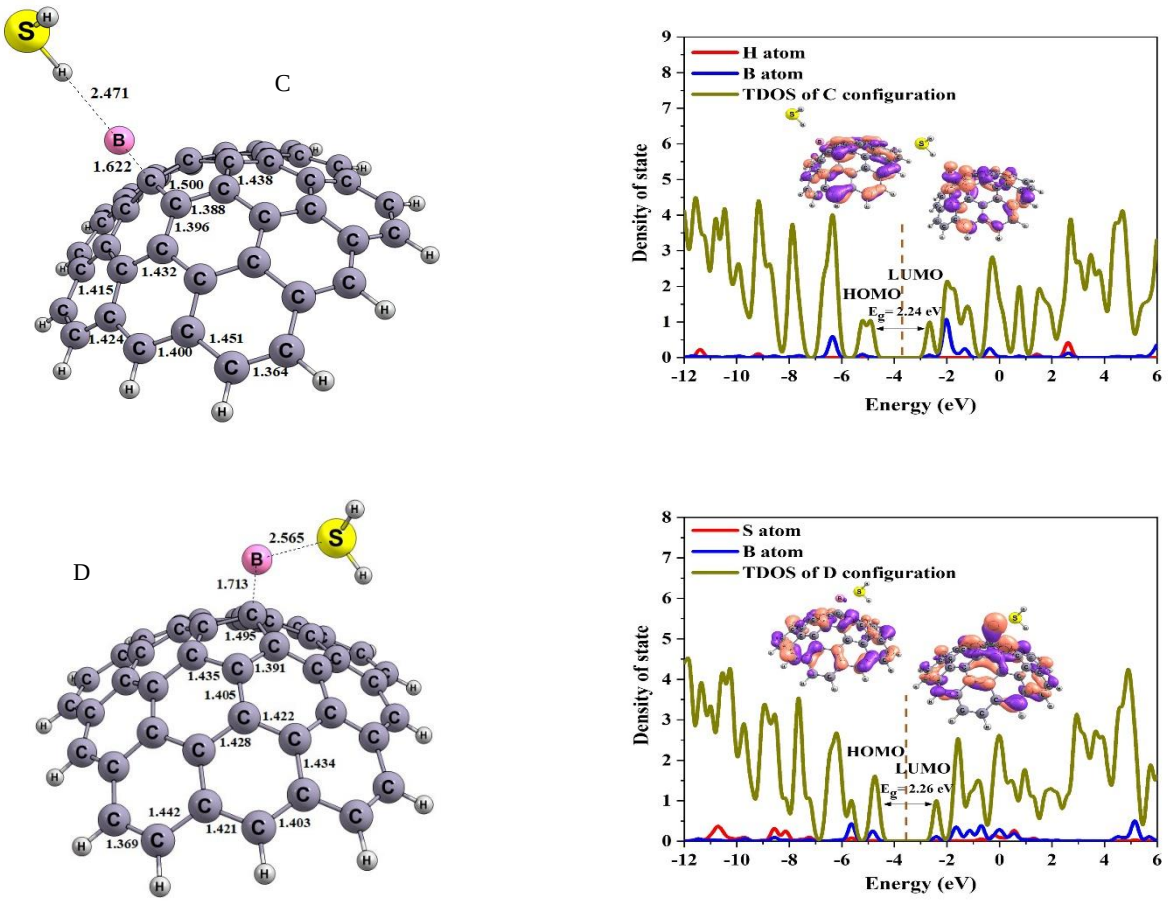

Fig. 10: The optimized structures, TDOS, and PDOS plots of the C and D configurations. All distances are in Å. The dashed line in PDOS plots indicates E_F.

From NCI-plot, the weak-inter-molecular-interactions can be clearly distinguished from the strong localized-inter-atomic-forces of attraction. The NCI-RDG also represents weak van der Waals interactions, destabilizing repulsive interactions, and stabilizing attractive interactions through green, red, and blue isosurfaces respectively. Moreover, intra and intermolecular weak interactions can be visualized by the appearance of spikes at different places on the electron density $\rho(\lambda_2)$ axis. The large -ve sign of $\rho(\lambda_2)$ in NCI analysis shows strong attractive forces, whereas $\rho(\lambda_2)$ value closer to zero represents weak van der Waals interactions. Strong repulsive non-bonded overlap, shown in red, indicates the regions with positive $(\lambda_2)\rho$, whereas the blue and green regions display attractive interactions and very weak interactions, respectively. Spikes are the spattering area of small ρ and 0∼medium RDG that introduce the weak interactions in complexes. According to Fig. 12, there are several spikes in the scatter plots of two configurations in B3LYP/6-311+G(d) level. In every region, more scatter points display larger electron density, that is, a larger contribution to the total interactions. The spike around 0 indicates the weak van der Waals forces of interaction, while the spike from larger 0.01 a.u. arises from the relatively strong interaction between the H_2S and CNC/B. In addition, the Spike with values smaller -0.01 a.u. arises from the strong repulsive interactions. From Fig.12, it is obvious that weak forces of interaction are exhibited between the H_2S gas and CNC/B structure, which can also be found in the color-filled inter-molecular isosurface image. The green regions between the H_2S and CNC/B illustrate van der Waals-type interactions, which are weak intermolecular forces. The blue color of the isosurface in the Fig. 12 shows a stabilization interaction. But it is not an absolute stabilizing interaction and because of its slightly red color. These weak interactions are quite advantageous due to the gas can easily be removed

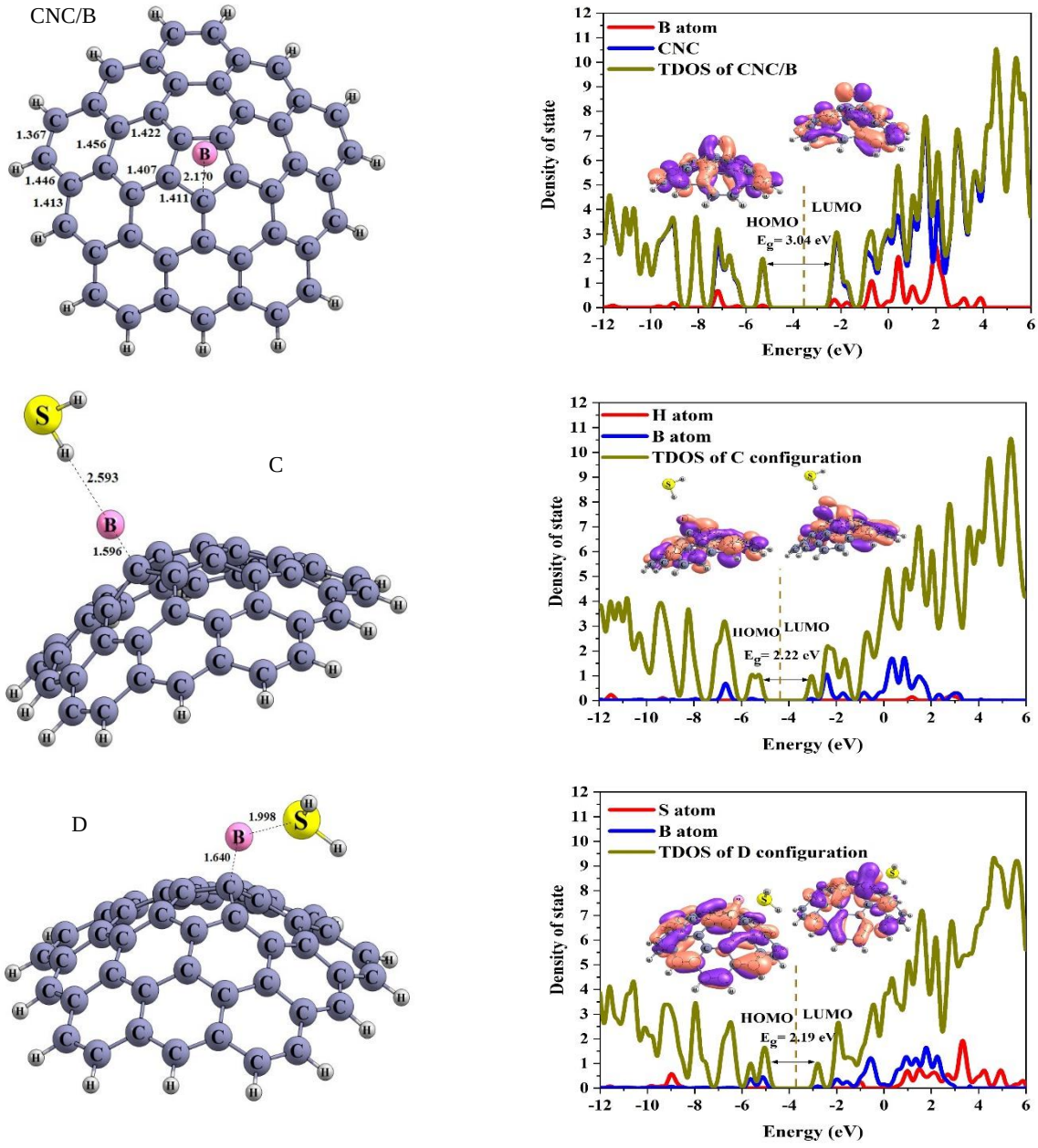

Fig. 11: The optimized structures, TDOS, and PDOS plots of the CNC/B, C, and D configurations in B3LYP/6-311+G(d) level. All distances are in Å. The dashed line in PDOS plots indicates E_F.

from the exterior surface of CNC/B to drain and recover the sensor.

Eventually, we concluded that CNC/B structure could be a potential sensor for the detection H_2s gas, and decorated with boron atom is a promising strategy.

MEP analysis

Fig. 13 shows the molecular electrostatic potential (MEP) surface of considered structures at the B3LYP/6-311+G(d) level of theory. The MEP distribution helps to determine the electrophilic and nucleophilic sites within a molecule. The regions with low MEP are characterized by the negative charge and are shown in red color in a typical ESP map. Conversely, the regions with high MEP, the positive charge, are shown with blue color. Fig. 13 shows that the electron density (red color) is localized on the B atom of CNC/B structure. Thus, H_2S gas should approach to the CNC/B through the B atom. As shown

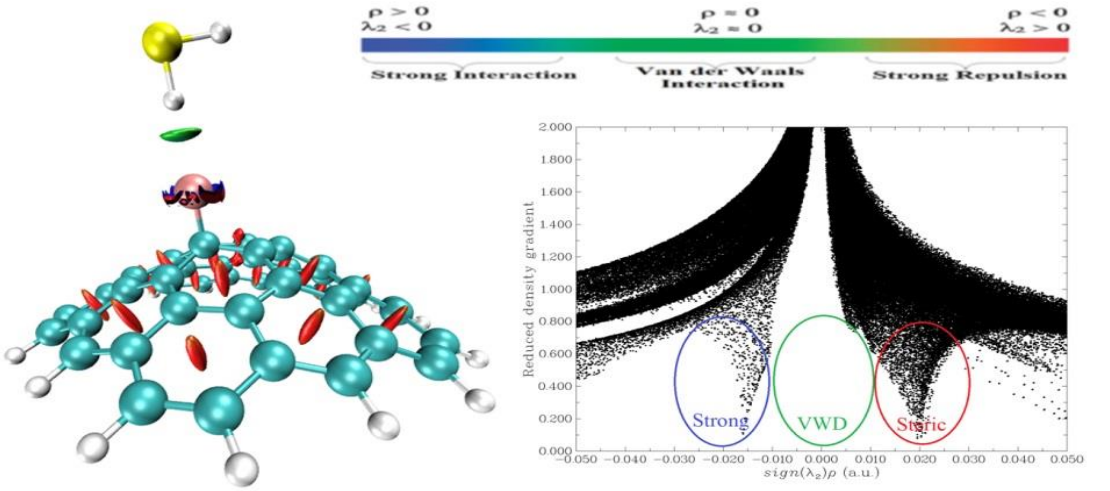

(C)

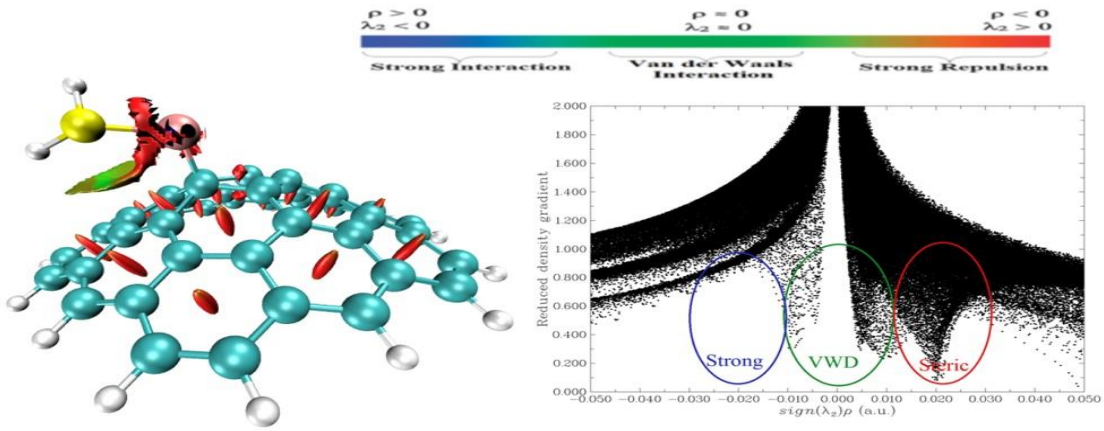

(D)

Fig. 12: Color-filled RDG isosurface maps (isovalue = 0.5 au) and plot of the RDG versus sign (λ_2)ρ for C, and D configurations.

in Fig. 13, the calculated MEP demonstrates that the positive charge (blue color) is located on the H_2S molecule (in D configuration) after the adsorption process, positive, confirming the donation of charge from the gas molecule to CNC/B structure. The negative perspective created on the B atom of the Cone/B structure is reasonable for the electrophilic attacking site. The data revealed that the CNC structure had a considerable positive electron density spread over its skeleton, indicating that CNC may be strongly linked to the B atom in CNC/N structure.

CONCLUSIONS

In the present study, the electrochemical sensing ability of CNC structure for H_2S gas is evaluated using DFT method. The DFT computed results show that H_2S was weakly adsorbed on the pristine CNC and it is not a good sensor. We applied several strategies to improve the adsorption ability on the surface of CNC including functionalizing with pyridinol and pyridinol oxide groups and decorating with some metals (M= B, Al, Ga, Mg, and Sc). The results illustrated that the strongest interaction is observed for CNC/B structure. The geometries of configurations reveal that H_2S gas adsorbed via H or S atom on the B of CNC/B structure. The E_{ads} of C and D configurations lie in range of -10.16 to -11.36 kcal/mom. NCI analysis confirms the presence of van der Waals interaction among H_2S and CNC/B, which is represented by the greencolor in RDG isosurfaces. NBO charge analysis reveals that the appreciable

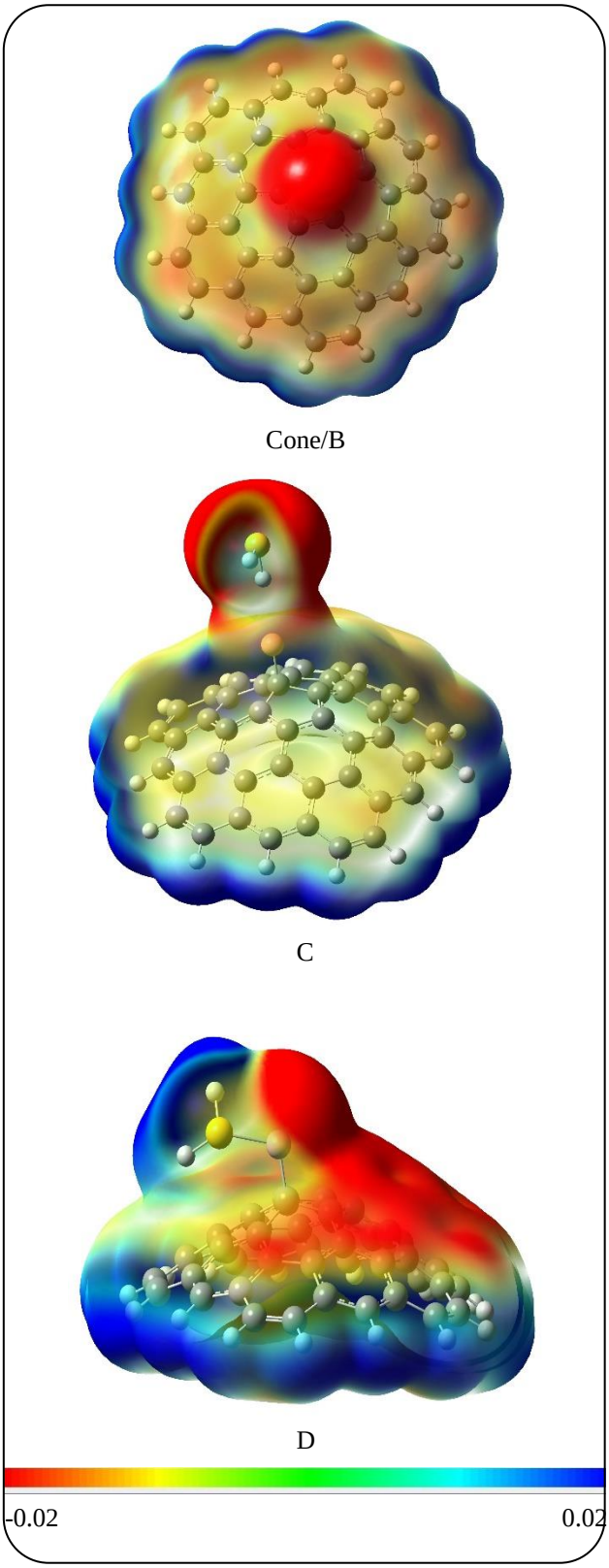

Fig. 13: MEP surface of the CNC/B, C, and D configurations. The surfaces are defined by the 0.0004 electrons/b3 contour of the electronic density.

charge transfer is noticed for D configuration (234 |me|). The highest charge transfer from CNC/B to H_2S gas is due to the lowest HOMO-LUMO energy gap. It is found that the electronic properties of CNC/B structure are much more sensitive to the presence of H_2S and might be used in H_2S chemical sensor. Totally, we concluded that CNC/B structure will be used in designing novel materials for potential applications to detect toxic H_2S gas.

Received : Nov. 26, 2022 ; Accepted : Apr. 3, 2023

REFERENCES

[1] Iijima S., Helical Microtubules of Graphitic Carbon, *Nature*, **354 (6348)**: 56-58 (1991).

[2] Lai P., Chen S., Lin M-F., Electronic Properties of Single-Walled Carbon Nanotubes under Electric And Magnetic Fields, *Physica E: Low-dimensional Systems and Nanostructures*, **40(6)**: 2056-2058 (2008).

[3] Song H-Y., Zha X-W., Mechanical Properties of Nickel-Coated Single-Walled Carbon Nanotubes and their Embedded Gold Matrix Composites, *Physics Letters A*, **374(8)**: 1068-1072 (2010).

[4] Beheshtian J., Ahmadi Peyghan A., Bagheri Z., Hydrogen Dissociation on Diene-Functionalized Carbon Nanotubes, *J. Mol. Model*, **19 (1)**: 255-261 (2013).

[5] Duan Y., Pirolli L., Teplyakov A.V., Investigation of the H_2S poisoning Process for Sensing Composite Material Based on Carbon Nanotubes and Metal Oxides, *Sens Actuators B*, **235**: 213-221 (2016).

[6] Yang R.T., Hydrogen Storage by Alkali-Doped Carbon Nanotubes–Revisited, *Carbon*, **38(4)**: 623-626 (2000).

[7] Li X., Zhou H., Fu C., Wang F., Ding Y., Kuang Y., A Novel Design of Engineered Multi-Walled Carbon Nanotubes Material and its Improved Performance in Simultaneous Detection of Cd (II) and Pb (II) by Square Wave Anodic Stripping Voltammetry, *Sens Actuators B*, **236**: 144-152 (2016).

[8] Ichihashi T., Ando Y., Pentagons, Heptagons and Negative Curvature in Graphite Microtubule Growth, *Nature*, **356(6372)**: 776-778 (1992).

[9] Krishnan A., Dujardin E, Treacy M., Hugdahl J., Lynum S., Ebbesen T., Graphitic Cones and the Nucleation of Curved Carbon Surfaces, *Nature*, **388(6641)**: 451-454 (1997).

[10] Ge M., Sattler K., Observation of Fullerene Cones, *Chem. Phys. Lett.*, **220 (3-5)**: 192-196 (1994).

[11] Kim Y., Hayashi T., Osawa K, Endo M., Dresselhaus M., Cone-Type Multi-Shell in the Hollow Core of Multi-Wall Carbon Nanotube, *Chem. Phys. Lett.*, **367(5-6)**: 537-540 (2003).

[12] Jordan S.P., Crespi V.H., Theory of Carbon Nanocones: Mechanical Chiral Inversion of a Micron-Scale Three-Dimensional Object, *Phys. Rev. Lett.*, **93(25)**: 255504 (2004).

[13] Grujicic M., Cao G., Gersten B., Enhancement of Field Emission in Carbon Nanotubes Through Adsorption of Polar Molecules, *Appl. Surf. Sci.*, **206(1-4)**:167-177 (2003).

[14] Saito Y., Tsujimoto Y., Koshio A., Kokai F., Field Emission Patterns from Multiwall Carbon Nanotubes with a Cone-Shaped Tip, *Appl. Phys. Lett.*, **90(21):** 213108 (2007).

[15] Guidotti T., Hydrogen Sulphide, *Occupational Medicine*, **46(5)**: 367-371 (1996).

[16] Greenwood N.N., Earnshaw A., "Chemistry of the Elements", Elsevier, (2012)

[17] Peyghan A.A., Omidvar A., Hadipour N.L., Bagheri Z., Kamfiroozi M., Can aluminum nitride nanotubes detect the toxic NH3 molecules?, *Physica E: Low-dimensional Systems and Nanostructures*, **44(7-8)**: 1357-1360 (2012).

[18] Trawka M., Smulko J., Hasse L., Granqvist C-G., Annanouch F.E., Ionescu R., Fluctuation Enhanced Gas Sensing with WO3-Based Nanoparticle Gas Sensors Modulated by UV Light at Selected Wavelengths, *Sens Actuators B*, **234**: 453-461 (2016).

[19] Eslami M., Vahabi V., Peyghan A.A., Sensing Properties of BN Nanotube Toward Carcinogenic 4-Chloroaniline: A Computational Study, *Physica E: Low-dimensional Systems and Nanostructures*, **76**: 6-11 (2016).

[20] Beheshtian J., Noei M., Soleymanabadi H., Peyghan A.A., Ammonia Monitoring by Carbon Nitride Nanotubes: A Density Functional Study, *Thin Solid Films*, **534**: 650-654 (2013).

[21] Ahmadi Peyghan A., Hadipour N.L., Bagheri Z., Effects of Al Doping and Double-Antisite Defect on the Adsorption of HCN on a BC2N Nanotube: Density Functional Theory Studies, *J. Phys. Chem. C*, **117(5)**: 2427-2432 (2013).

[22] Hong Y., Kim C-H., Shin J., Kim K.Y., Kim J.S., Hwang C.S., Lee J-H., Highly Selective ZnO Gas Sensor Based on MOSFET Having a Horizontal Floating-Gate, *Sens Actuators B*, **232**: 653-659 (2016).

[23] Solimannejad M., Kamalinahad S., Shakerzadeh E. Sensing Performance of Sc-Doped B12N12 Nanocage for Detecting Toxic Cyanogen Gas: A Computational Study, *Physical Chemistry Research*, **4(3)**: 315-332 (2016).

[24] Vakili M., Bahramzadeh V., Vakili M., A Comparative Study of SCN-Adsorption on the Al12N12, Al12P12, and Si and Ge-Doped Al12N12 Nano-Cages to Remove from the Environment, *Journal of Chemistry Letters*, **1(4)**: 172-178 (2020).

[25] Vessally E., Siadati S.A., Hosseinian A., Edjlali L., Selective Sensing of Ozone and the Chemically Active Gaseous Species of the Troposphere by Using the C20 Fullerene and Graphene Segment, *Talanta*, **162**: 505-510 (2017).

[26] Arshadi S., Abdolahzadeh F., Vessally E., Butadiyne-Linked Porphyrin Nanoring as a Highly Selective O_2 Gas Sensor: A Fast Response Hybrid Sensor, *Journal of Molecular Graphics and Modelling*, **119**: 108371 (2023).

[27] Khalif M., Daneshmehr S., Arshadi S., Söğütlü İ., Mahmood E.A., Abbasi V., Vessally E., Adsorption of O_2 Molecule on the Transition Metals (TM (II)= Sc^{2+}, Ti^{2+}, V^{2+}, Cr^{2+}, Mn^{2+}, Fe^{2+}, Co2+, Ni^{2+}, Cu^{2+} and Zn^{2+}) Porphyrins Induced Carbon Nanocone (TM (II) PCNC), *Journal of Molecular Graphics and Modelling*, **119**: 108362 (2023).

[28] Solimannejad M., Kamalinahad S., Shakerzadeh E., Sensing Performance of Sc-Doped $B_{12}N_{12}$ Nanocage for Detecting Toxic Cyanogen Gas: A Computational Study, *Physical Chemistry Research*, **4(3)**: 315-332 (2016).

[29] Solimannejad M., Kamalinahad S., Shakerzadeh E., Selective Detection of Toxic Cyanogen Gas in the Presence of O_2, and H_2O Molecules Using a AlN Nanocluster, *Physics Letters A*, **380(36)**: 2854-2860 (2016).

[30] Rahimi R., Kamalinahad S., Solimannejad M., Adsorption of Rare Gases on the C20 Nanocage: A Theoretical Investigation, *Materials Research Express*, **5(3)**: 035006 (2018).

[31] Kamalinahad S., Solimannejad M., Shakerzadeh E., Sensing of Ozone (O_3) Molecule Via Pristine Singe-Walled Aluminum Nitride Nanotube: A DFT Study, *Superlattices Microstruct*, **89**: 390-397 (2016).

[32] Nazar Ali Z., Ahmadi S.A., Ghazanfari D., Sheikhhosseini E., Razavi R., Investigation of Flutamide@ Ethyleneimine as Drug Carrier by Nanocone and Nanotube Theoretically, *Iranian Journal of Chemistry and Chemical Engineering (IJCCE)*, **41(10)**: 3275-3281 (2021)

[33] Tavakoli S., Ahmadi S.A., Ghazanfari D., Sheikhhosseini E., Theoretical Investigation of Functionalized Fullerene Nano Carrier Drug Delivery of Fluoxetine, *Journal of the Indian Chemical Society*, **99(7)**: 100561 (2022).

[34] Najibzade Y., Sheikhhosseini E., Akhgar M.R., Ahmadi S.A., Absorption of Tranylcypramine on C60 Nanocage: Thermodynamic and Electronic Properties, *Pakistan Journal of Pharmaceutical Sciences*, **35(3)**: 815-818 (2022).

[35] Sabzehmeidani M.M., Mahnaee S., Ghaedi M., Heidari H., Roy V.A., Carbon Based Materials: A Review of Adsorbents for Inorganic and Organic Compounds, *Materials Advances*, **2(2)**: 598-627 (2021).

[36] Söğütlü İ., Arshadi S., Mahmood E.A., Abbasi V., Kamalinahad S., Vessally E., In silico Investigation of Metalophthalocyanine Substituted in Carbon Nanocones (TM-PhCCNC, TM= Sc^{2+}, Cr^{2+}, Fe^{2+} and Zn^{2+}) as a Promising Sensor for Detecting N_2O Gas Involved in Covid-19, *Journal of Molecular Structure*, **1284(15)**: 135263 (2023).

[37] Salih E., Ayesh A.I., DFT Investigation of H_2S Adsorption on Graphenenanosheets and Nanoribbons: Comparative Study, *Superlattices Microstruct*, **146**: 106650 (2020).

[38] Deji R., Choudhary B., Sharma R.K., Hydrogen Sulfide Gas Sensor Using Osmium Doped Graphene Nanoribbon: An Insights from DFT Study, *Materials Letters*, **306**: 130986 (2022).

[39] Salih E., Ayesh A.I., Co-Doped Zigzag Graphene Nanoribbon Based Gas Sensor for Sensitive Detection of H_2S: DFT Study, *Superlattices Microstruct*, **155**: 106900 (2021).

[40] Srivastava R., Suman H., Shrivastava S., Srivastava A., DFT Analysis of Pristine and Functionalized Zigzag CNT: A Case of H_2S Sensing, *Chem. Phys. Lett.*, **731**: 136575 (2019).

[41] Suman H., Srivastava R., Shrivastava S., Srivastava A., Jacob A., Malvi C., DFT Analysis of H_2S Adsorbed Zigzag and Armchair Graphene Nanoribbons, *Chem. Phys. Lett.*, 745:137280 (2020).

[42] Mori-Sunchez P., Cohen A., Yang W., Discontinues Nature of the Exchangecorrelation Functional in Strongly Corrected System, *Phys. Rev. Lett.*, **102**: 066403-0066408 (2009).

[43] Schmidt M.W., Baldridge K.K., Boatz J.A., Elbert S.T., Gordon M.S., Jensen J.H., Koseki S., Matsunaga N., Nguyen K.A., Su S., General Atomic and Molecular Electronic Structure System, *J. Comput. Chem.*, **14(11)**: 1347-1363 (1993).

[44] Baei M.T., Adsorption Properties and Quantum Molecular Descriptors of OCN^- Adsorbed on (6, 0),(7, 0), and (8, 0) Zigzag Single-Walled Boron Nitride Nanotubes: A Computational Study, *Monatsh. Chem.*, **143(7)**: 989-995 (2012).

[45] Hizhnyi Y., Nedilko S., Borysiuk V., Shyichuk A., Ab Initio Computational Study of Chromate Molecular Anion Adsorption on the Surfaces of Pristine and B-or N-Doped Carbon Nanotubes and Graphene, *Nanoscale Research Letters*, **12(1)**: 1-9 (2017).

[46] Vessally E., Behmagham F., Massoumi B., Hosseinian A., Edjlali L., Carbon Nanocone as an Electronic Sensor for Hcl Gas: Quantum Chemical Analysis, *Vacuum*, **134**: 40-47 (2016).

[47] Hadipour N.L., Ahmadi Peyghan A., Soleymanabadi H., Theoretical Study on the Al-doped ZnO Nanoclusters for CO Chemical Sensors, *J. Phys. Chem. C*, **119(11)**: 6398-6404 (2015)

[48] Craciun M., Khrapach I., Barnes M., Russo S., Properties and Applications of Chemically Functionalized Graphene, *Journal of Physics: Condensed Matter*, **25(42)**: 423201 (2013).

[49] Bekyarova E., Kalinina I., Sun X., Shastry T., Worsley K., Chi X., Itkis M.E., Haddon R.C., Chemically Engineered Single-Walled Carbon Nanotube Materials for the Electronic Detection of Hydrogen Chloride, *Adv. Mater.*, **22(7)**: 848-852 (2010).

[50] Seenithurai S., Pandyan R.K., Kumar S.V., Saranya C., Mahendran M., Al-Decorated Carbon Nanotube as the Molecular Hydrogen Storage Medium, *Int. J. Hydrogen Energy*, **39(23)**: 11990-11998 (2014).

[51] Amaniseyed Z., Tavangar Z., Hydrogen Storage on Uncharged and Positively Charged Mg-Decorated Graphene, *Int. J. Hydrogen Energy*., **44(7)**: 3803-3811 (2019).

[52] Cui S., Zhao N., Shi C., Feng C., He C., Li J., Liu E., Effect of Hydrogen Molecule Dissociation on Hydrogen Storage Capacity of Graphene with Metal Atom Decorated, *J. Phys. Chem. C*, **118(2)**: 839-844 (2014).

[53] Chen X., Gao P., Guo L., Wen Y., Fang D., Gong B., Zhang Y., Zhang S., High-Efficient Physical Adsorption and Detection of Formaldehyde Using Sc-and Ti-Decorated Graphdiyne, *Physics Letters A*, **381(9)**: 879-885 (2017).

[54] Johnson E.R., Keinan S., Mori-Sánchez P., Contreras-García J., Cohen A.J., Yang W., Revealing Noncovalent Interactions, *J. Am. Chem. Soc.*, **132(18)**: 6498-6506 (2010).